Engineering Structures 271 (2022) 114956

Contents lists available at ScienceDirect

Engineering Structures

journal homepage: www.elsevier.com/locate/engstruct

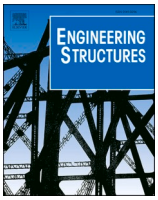

Experiments on cyclic behaviour of cold-formed steel-rubberised concrete semi-rigid moment-resisting connections

Alireza Bagheri Sabbagh [a,*], Naeimeh Jafarifar [b], Paul Davidson [a], Kanan Ibrahimov [a]

[a] School of Engineering, University of Aberdeen, Scotland, UK
[b] School of Architecture and Built Environment, Robert Gordon University, Scotland, UK

ARTICLE INFO

Keywords:
Cold-formed steel
Moment-resisting connections
Semi-rigid joints
Cyclic loading

ABSTRACT

This paper presents the results of full-scale physical tests on a recently developed cold-formed steel (CFS) semi-rigid moment-resisting connection infilled with rubberised concrete (RuC) for seismic application. The connection comprises side-plates attached to both sides of built-up tubular CFS beam and column sections through either screwed or welded connections. The tests were performed on both bare steel and CFS-RuC composite connections under cyclic loading for comparison purposes. The predominant modes of failure are beam local buckling and side plate plasticity in the bare steel connections and screw shear failure in the composite connections. The results show that the composite connection typically reaches 45% higher strength and 21% greater energy dissipation capacity than the bare steel connection both having 24 screw arrays. These indicate the beneficial effects of the infill RuC in prevention of the beam local buckling in connections with identical connection configuration. The energy dissipation capacity of the bare steel connection having 36 screw arrays, however, was 70% greater than that of the composite connection with 24 screw arrays. This reflects side plate plasticity being a more effective energy dissipation mechanism than the other identified mechanisms.

1. Introduction

Buildings and construction are responsible for nearly 40 % of all global CO_2 emissions each year, around 10 % of which are directly related to steel structures [1]. This suggests a need for more efficient usage of steel components in building structures, and that improving structural performance can make an important contribution to the reduction of global carbon emissions. Lightweight steel framing (LSF) structures made of cold-formed steel (CFS) sections can offer a cost-effective and low carbon structural solution with ease of prefabrication and offsite construction compared with the heavier hot-rolled steel frames [2]. The best-practice LSF systems comprise stud walls and joisted floors having simply supported floor-to-wall connections, typically governed by the mid-span deflection and premature local failure limit states, which could lead to under-utilised joist and stud sections [3,4]. To address these identified deficiencies a semi-rigid moment-resisting floor-to-wall connection has been recently developed by the first author [5] which can lead to an improved utilisation and a more efficient design of stud-wall systems.

Besides the ongoing research on stud-wall systems, a bolted CFS moment-resisting (MR) connection has also been developed for a framed/skeleton type of LSF systems [6–13]. The developed connection fulfils the requirements of highly ductile moment frames [14–15] through the beam plasticity and a bolting friction-slip mechanism whilst local buckling is postponed by using folded flange beam sections and transverse stiffeners. This connection has been further investigated by other research groups mainly focusing on optimisation of the connection bolting configuration and the CFS beam section [16–18]. Other types of CFS bolted moment-resisting connections have been developed and tested for portal frame systems [19].

More recently another type of CFS MR connection has been developed by the first author (see Fig. 1 for the detailing) [20], based on finite element (FE) investigation, comprising tubular built-up beam and column hollow sections with the same overall width infilled with rubberised concrete (RuC). This detailing could postpone the beam local buckling through the restraining effect of the infilled RuC achieving a strength level greater than the nominal moment capacity of the beam section [20]. For this connection, side plates can be welded offsite to the column and screwed onsite to the beam, as shown in Fig. 1, like the well-known column-tree type of connections in hot-rolled steel MR framing counterpart. The side plates are welded to the opposite faces of the column through flare groove weld lines filling the rounded space

* Corresponding author.
E-mail addresses: alireza.bsabbagh@abdn.ac.uk (A. Bagheri Sabbagh), n.jafarifar@rgu.ac.uk (N. Jafarifar).

https://doi.org/10.1016/j.engstruct.2022.114956
Received 17 May 2022; Received in revised form 20 August 2022; Accepted 9 September 2022
Available online 18 September 2022

between the side plate's inner surface and the channel corners. Both the beam and column tubular sections are built-up using un-lipped channel sections connected to one another through their top and bottom flanges using overlapped screwed or welded connections. The choice of infill RuC has been adopted to replace mineral aggregates of normal concrete by rubber particles recycled from waste tyres, thus a more sustainable construction solution [20].

The experimental study presented herein investigates the cyclic behaviour of the developed CFS-RuC beam-to-column MR connection through full-scale physical testing. Both bare steel and composite CFS-RuC connections producing various failure modes within the connection components have been tested for comparison purposes. This determines the cyclic loading effects on the hysteretic behaviour of such connections.

2. Testing arrangement and design considerations

Fig. 2 shows a sketch and a photo of the set-up of the full-scale CFS-RuC beam-to-column connection tests conducted at the University of Aberdeen. The testing specimens comprise a 2 m long cantilever beam connected to a 1.5 m high stub column through side plate screwed connection. This testing arrangement represents a 4 m span moment-frame delineated at the beam mid-span inflection point under lateral loading condition. It should be noted that the intention of the proposed testing arrangement is to investigate the beam-to-side plate connection behaviour under cyclic lateral loading condition and that the axial behaviour of the column is not the focus of this research. The side plates are connected to the side faces of the beam and column through 24 or 36 arrays of #S-MD 5.5 × 2.5 self-drilling Hilti screws with 5.4 mm shaft diameter (labelled as 24#12 or 36#12) and flare groove welded lines, respectively. As can be seen in Fig. 2 the testing specimen is fixed to a supporting frame comprising a strong hot-rolled steel column supported by a diagonal brace. The strong column is fixed to a concrete strong floor through a base plate and a set of base rails (see the photo in Fig. 2) providing a rigid base connection. Two bearing plates having 20 mm thickness were used to fix the CFS column to the supporting column through four M20 long rods at the top and bottom points. Top and bottom filler plates were placed at the gap between the specimen and supporting column welded to the CFS column and bolted to the strong column. The detailing for the CFS column connection to the supporting strong column should resist the top and bottom shear forces created by a hydraulic actuator at the free end of the beam (see Fig. 2) supported by a reaction frame. The actuator loading was applied at a distance of 2040 mm from the connection centroid through a hinge connection. The hinge comprised a shackle head, a swinging link and a pivot shaft attached to two 20 mm thickness L-shaped plates which were connected to the beam using five M20 rods (See the sketch in Fig. 2). Two box columns were placed at either side of the beam with a small gap filled with PTFE sheets providing a frictionless lateral bracing restraint to avoid any possible global instability.

The beam and column tubular sections comprised two un-lipped channels having a web height of 300 mm connected to one another through their 100 mm width top and bottom flanges with an overlapped width of 25 mm using self-drilling screws to form a rectangular hollow section. The beam hollow sections had either 2 mm or 3 mm thicknesses with an overall width of 175 mm (respectively labelled by CFS300-175-2 and CFS300-175-3), connected to a column hollow section with 4 mm thickness (CFS300-175-4). The same height of 300 mm has been assumed for the side plates with 4 mm thickness and 620 mm width accommodating the screw fasteners to the beam and the welded lines at the opposite faces of the column. For the composite connection, the beam and column hollow sections were filled by RuC through the filling holes on the mid-height of the side of the sections as can be seen in the test photo in Fig. 2. The steel grade of S275 has been utilised for all the steel components having the nominal yield strength of $f_y = 275$ MPa, the elastic modulus of $E = 203500$ MPa and the Poisson's ratio of $\nu = 0.33$. Based on the Direct Strength Method (DSM) equations, prescribed in Appendix 1 of the North American Specification AISI S100 [21], the nominal bending moment (M_n) values for the 2 mm and 3 mm beam sections were $M_n = 33$ kN m and 64 kN m, respectively accounting for local/distortional buckling modes of failure. The elastic buckling loads inputted into DSM equations have been calculated using CUFSM finite strip method software [22].

For the composite connection specimens, the characteristic compressive strength of the RuC infill having 35 % rubber content based on standard cylinder compression loading tests was around $f_{rc} = 12$ MPa. It should be noted that the moment strength contribution of the infilled RuC in the composite beam has been ignored due to a crack propagation which could be expected at both sides of the beam under cyclic loading. It has also been assumed that the confining pressure on the tubular sections becomes insignificant due to the relatively large width-to-thickness ratio (greater than 15) of the sectional elements, according to a numerical work on concrete-filled steel box sections reported in [23]. Therefore, providing a restraining effect to the beam and column

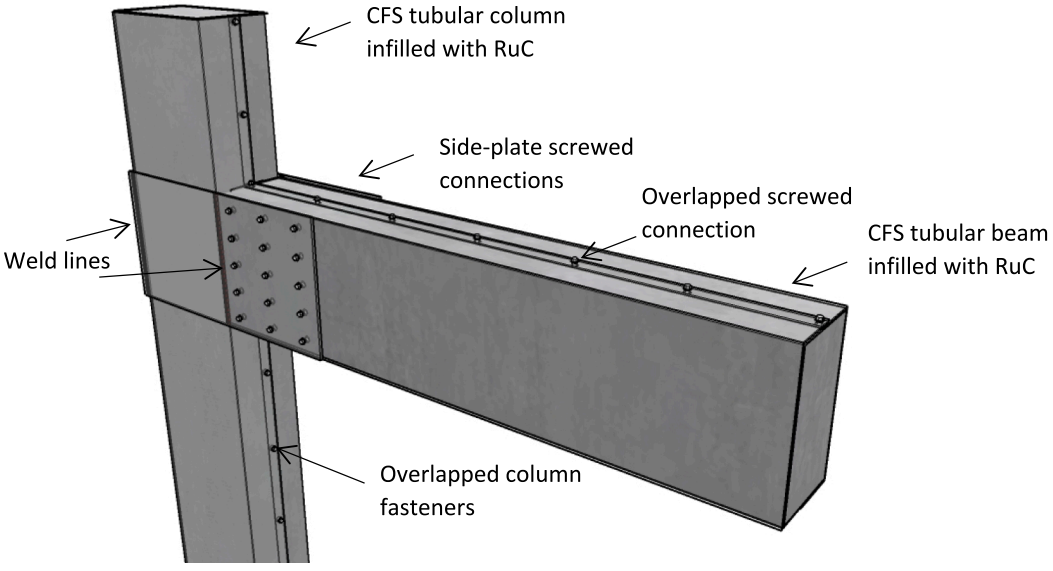

Fig. 1. Schematic view of the developed composite cold-formed steel (CFS)- rubberised concrete (RuC) moment-resisting screwed connection.

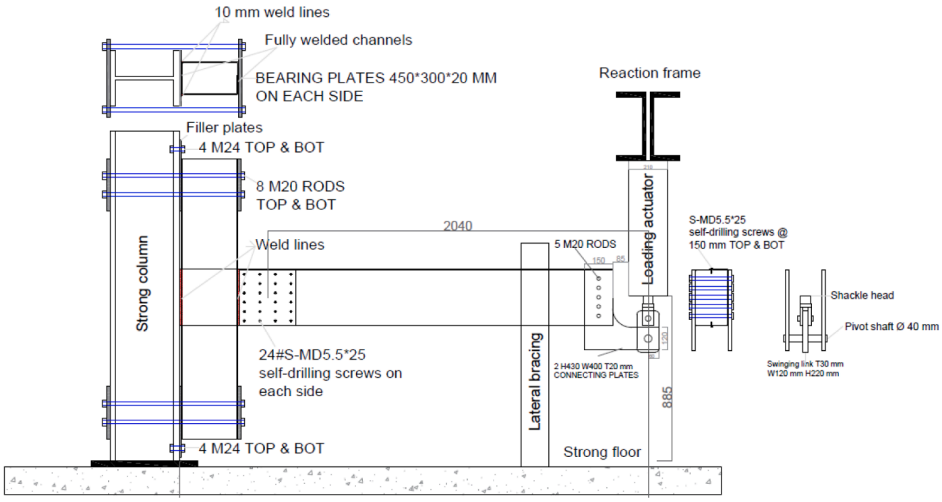

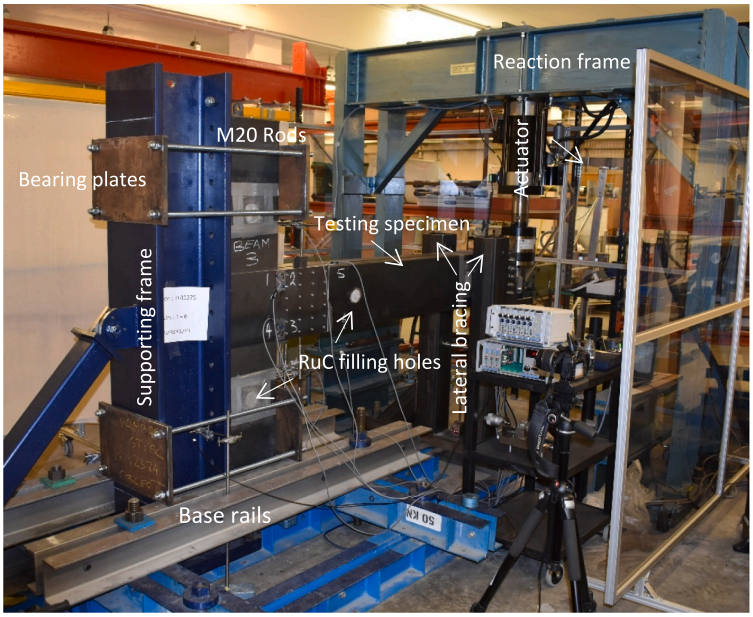

Fig. 2. A sketch and a photo of the test set-up at the University of Aberdeen.

steel hollow sections is assumed to be the main function of the infilled RuC for the testing specimens.

Table 1 contains the testing connection configurations and the associated governing limit states including the beam local buckling (BLB), ultimate screw shear (USS) and side plate plasticity (SPP), identified through the accompanying FE investigation reported in [20]. The connections are labelled as CFS2-4-SP4#24, CFS3-4-SP4#36 and CFSRuC2-4-SP4#24, standing for the bare steel and composite connection acronyms followed by the beam thicknesses of 2 mm or 3 mm, the column thickness of 4 mm, the side plate (SP) thickness of 4 mm and the screw arrays of 24#12 or 36#12. These three sets of connection configurations have been chosen to capture the three predicted limit states (i.e., BLB, USS and SPP). These connections were designed to behave such that BLB would govern the bare steel CFS2-4-SP4#24 connection, while USS would be the predominant mode of failure for the composite CFSRuC2-4-SP4#24 connection along with a degree of SPP. By increasing the number of screws from 24#12 to 36#12 in the bare steel CFS3-4-SP4#36 connection, SPP would become the dominant limit

Table 1
Testing connections and predicted governing limit states.

Testing connections	Testing configuration				Governing limit states*		
	Beam section	Column section	Side plate dimension (mm)	Screw array	BLB	USS	SPP
CFS2-4-SP4#24	CFS300-175-2	CFS300-175-4	620 × 300 × 4	24#12	√	–	–
CFSRuC2-4-SP4#24	CFS300-175-2	CFS300-175-4	620 × 300 × 4	24#12	–	√	√
CFS3-4-SP4#36	CFS300-175-3	CFS300-175-4	620 × 300 × 4	36#12	–	–	√

* BLB: beam local buckling, USS: ultimate screw shear, SPP: side plate plasticity

state. The beam-to-side plate screw connection has been designed based on the yielding and ultimate capacities of $P_{nys} = 7$ kN and $P_{nus} = 10.91$ kN taken from [24] for an identical #12 steel-to-steel connection screw fastener. The column section and the welded lines of the side plate-to-column connection both remain elastic complying with the well-known strong-column-weak beam concept in seismic-resistant moment frames.

2.1. Instrumentation

Fig. 3 shows a photo of strain gauges SG1- SG6 mounted on the critical points of the testing specimens to capture the predicted SPP and BLB via the sets of SG1-SG4 and SG5-SG6, respectively. The set of SG1-SG4 were positioned at the side plate section adjacent to the face of the column while SG5-SG6 were placed at the beam top and bottom flanges just after the side plate connection. Fig. 3 also shows the displacement transducers DT1 and DT2 located on the beam top and bottom flanges at the connection centroid and pointed to the column face to measure the relative rotation between the beam and column. This can be calculated using $(D_1\text{-}D_2)/d$, where D_1 and D_2 are the measured displacements by the transducers and d is the distance between the transducers (see Fig. 3). The obtained beam-column relative rotations have been used to assess the connection rigidity as discussed herein under section 3.4.

2.2. Loading protocol

Fig. 4 shows the loading hinge connection connected to the L-shaped plates through which a cyclic loading was applied following the AISC Seismic Provision [15] for qualifying beam-column moment-resisting connections. Fig. 5 shows the number of loading cycles for each of the specified connection rotations of θ from initial elastic cycles to the plastic cycles which can be continued at 10 mrad intervals until a significant strength degradation. The actuator displacement can be calculated based on a given θ multiplied by the distance of 2040 mm measured from the loading point to the connection centroid.

3. Test results

The normalised moment-rotation (M/M_n - θ) hysteretic curves of the tested bare steel and composite connections as well as the energy dissipation, strain gauge and connection rigidity results are presented in the following subsections. The beam bending moment, M, has been

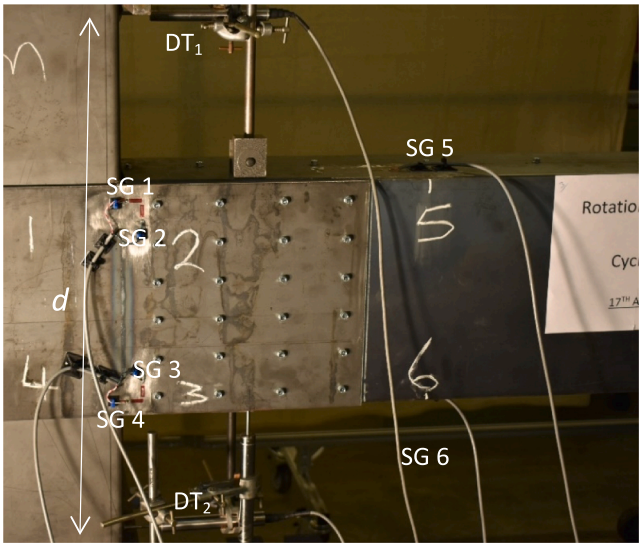

Fig. 3. Strain gauges (SG1-SG6) and displacement transducers (DT1-DT2) mounted on the testing specimens.

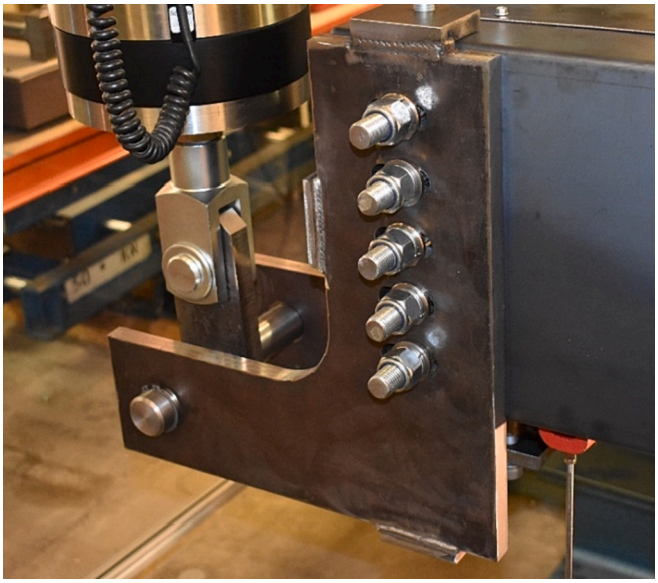

Fig. 4. Loading hinge connection.

calculated at the connection end distanced at 1890 mm from the loading point where BLB could occur, in the bare steel connections, at around the nominal moment of M_n.

3.1. Hysteretic behaviour of the testing connections

Fig. 6 shows the M/M_n - θ hysteretic curves for all the tested bare steel and composite connections listed in Table 1 (i.e., CFS2-4-SP4#24, CFS3-4-SP4#36 and CFSRuC2-4-SP4#24). As can be noticed two identical composite connections have been tested with the only difference being the beam channels welded together (labelled by CFSRuC2-4-SP4#24 (w)), as another fabrication method for the beams, instead of the screwed fasteners. As can be observed the initial elastic cycles have been followed by the plastic cycles respectively identified by AB and BCD regions, in the downstroke loading direction. It should be noted that, in the upstroke loading direction, the cyclic loading has been affected by a degree of a set-up slackness in that direction. The test set-up has been modified for the CFS3-4-SP4#36 and CFSRuC2-4-SP4#24 (w) connections to mitigate the slackening effect. As a result, the hysteretic curves of these connections, as seen in Fig. 6, were relatively more symmetrical, as expected.

In the CFS2-4-SP4#24 bare steel connection, the beam local buckling (BLB) initiated at point B around 10 mrad rotation which has been intensified and reached the peak moment of 0.97 M_n at point C (where $M_n = 33$ kN m). This has been followed by a relatively smooth strength degradation over the CD region after the initial sharp load drop which occurred immediately after point C. Fig. 7 (a) shows the beam flange local buckling, as the predominant mode of failure in the bare steel connection, which has been initiated around point B, intensified around point C and eventually extended to the beam web plates around point D.

The two identical composite connections (CFSRuC2-4-SP4#24 and CFSRuC2-4-SP4#24(w)) produce a pinching-type hysteretic behaviour which also matches the model characterised through the lap-joint tests by Tao et al. [24]. The flat portions in the hysteretic curves are associated with the slotted holes created as the screws bear against the plates during the cyclic loading. As can be realised the downstroke loading hysteretic curves of both composite connections are identical. The screw shear failure limit state governed the hysteretic behaviour of the composite connections initiated at point B around 10 mrad rotation (see Fig. 6) through yielding of the screws which led to a lower connection stiffness over the BC region. This eventually caused the ultimate screw shear (USS) failure around point C, respectively corresponding to the

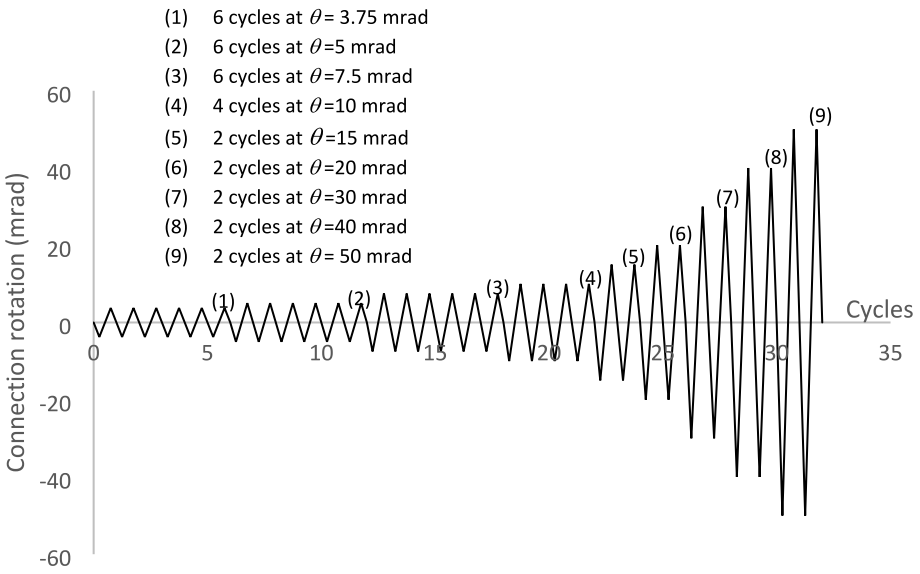

Fig. 5. Loading cycles.

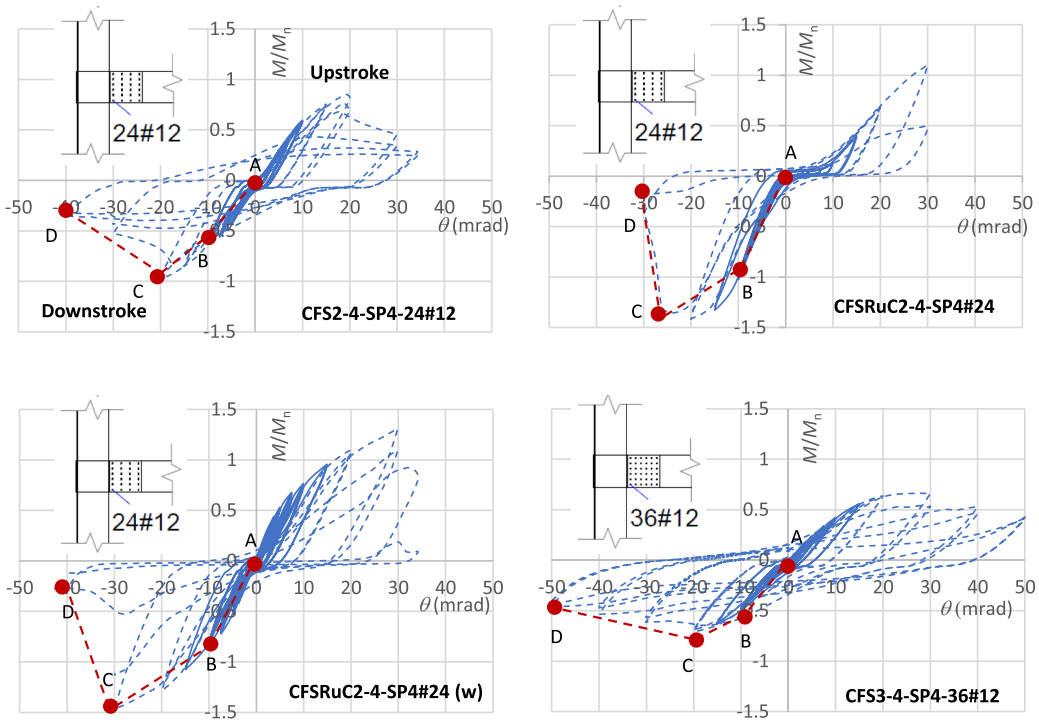

Fig. 6. Hysteretic moment-rotation curves of CFS2-4-SP4#24, CFSRuC2-4-SP4#24 and CFS3-4-SP4#36 connections.

peak moment of around 1.41 M_n and 1.46 M_n (where M_n = 33 kN m) in both the composite connections which are reasonably close values, as expected. The progression of the screw shear failure led to a sharp strength degradation over the CD region. This initiated at the corner screws and progressed towards the centre and middle screws complying with the theoretical uniform connection rotation. The elimination of the beam local buckling indicates the effectiveness of the infilled RuC which resulted in achievement of 45 % greater moment strength in the composite connection compared with that of the corresponding bare steel connection (i.e., CFS2-4-SP4#24). Fig. 7 (b) shows a side and a top view of the connection deformation and failure due to the screw shear limit state at point D. This can be recognised when comparing the relative rotation between the beam and the side plate through the white line which was initially located along the vertical edge of the side plate on the beam.

It should be noted that in the above bare steel and composite connection tests the upstroke rotation was limited to 35 mrad which was slightly lower than 40 mrad specified by the loading protocol. This was due to a limitation in the actuator movement in the upstroke loading direction and since these connections already failed in the earlier rotations it was decided not to go up to the value of 40 mrad to avoid possible damages in the actuator. This limitation, however, was checked and modified for the CFS3-4-SP4#36 connection test for which a larger rotation was expected.

In the CFS3-4-SP4#36 bare steel connection, the side plate plasticity (SPP) was the predominant mode of failure which led to a relatively

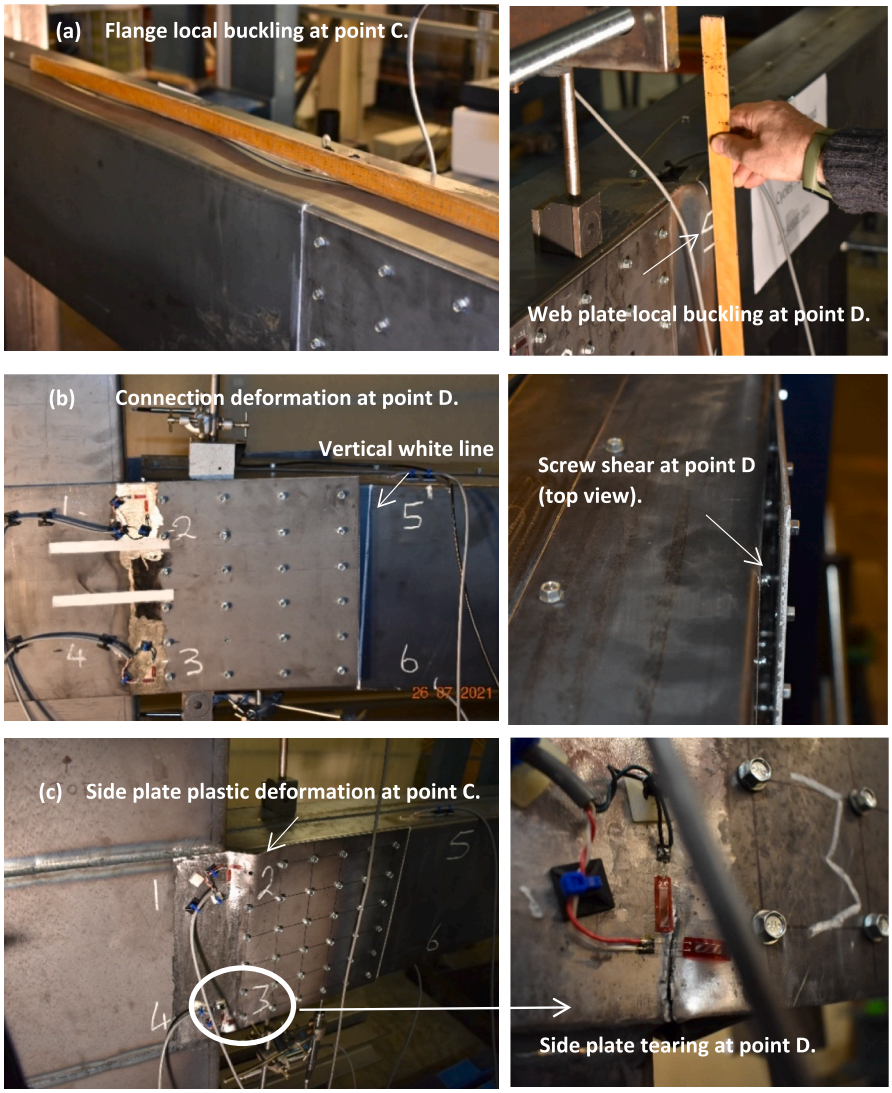

Fig. 7. Predominant mode of failures in the (a) CFS2-4-SP4#24, (b) CFSRuC2-4-SP4#24 and (c) CFS3-4-SP4#36 connections.

wider hysteretic behaviour (see Fig. 6) than that of the composite connection affected by the pinching behaviour. Fig. 7 (c) shows a plastic deformation of the side plate developed at the face of the column. This corresponds to the beam peak moment of 0.7 M_n (around point C) where M_n is the nominal moment strength of the 3 mm beam section (i.e., M_n = 64 kN m). This has been followed by a relatively smooth strength degradation over the CD region over which the side plate plastic hinge deformation has been intensified and eventually led to a tearing failure (see Fig. 7 (c)) at the side plate around point D. This occurred adjacent to the side plate-to-column weld lines which prevented propagation of the plastic deformation to the column side of the connection. The connection rotation at the failure point D reached 50 mrad which is greater than those of the bare steel and composite connections failed through BLB, and USS discussed above.

It is worth mentioning that, as expected, no relative deformation and damage were observed between the CFS column and the strong supporting frame. Further, since the column panel zone and the welded lines were designed conservatively to remain elastic, the instrumentation was set to capture the relative rotation between the beam and the column face which determines the connection rigidity (discussed under section 3.4).

3.2. Strain gauge results of the tested connections

Fig. 8 shows the maximum strain gauge values at the critical sections of the side plate (SG1-SG4) and the beam top and bottom flanges (SG5-SG6) at each loading cycle for CFS2-4-SP4#24, CFSRuC2-4-SP4#24 (w) and CFS3-4-SP4#36 connections. As can be seen the strain values of SG1 and SG4 (i.e., the horizontal strain gauges) in all the bare steel and composite connections have exceeded the assumed proof yielding strain value of ε_y = 2000 μs. A higher level of plasticity occurred in the side plate of the CFSRuC2-4-SP4#24 and CFS3-4-SP4#36 connections, as expected, which initiated around 10 mrad rotation and sharply exceeded 10000 μs at around 20–30 mrad (corresponding to points B and C in Fig. 6, respectively).

The strain values of the beam top and bottom flanges of the CFS2-4-SP4#24 connection (i.e., SG5-SG6) have been significantly affected by the flange local buckling around 20 mrad onwards (corresponding to CD region in Fig. 6). In the CFSRuC2-4-SP4#24 and CFS3-4-SP4#36 connections, however, the beam strain barely exceeded the yielding value at around point C in their corresponding hysteretic curves.

3.3. Energy dissipation of the tested connections

Fig. 9 shows the cumulative energy dissipation (E) of the composite and bare steel connections calculated at each cycle based on the areas

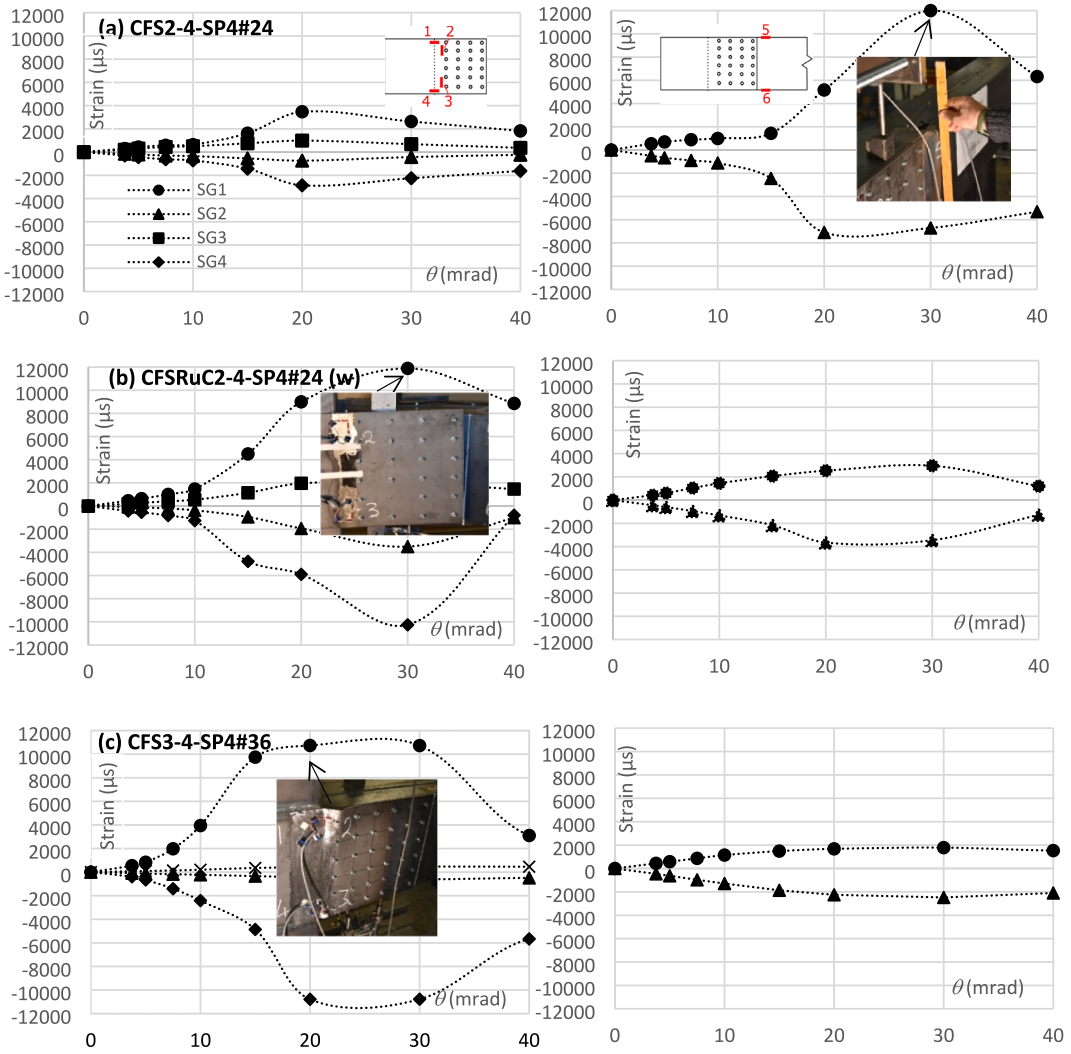

Fig. 8. Maximum strain gauge values of SG1-SG6 at the side plate and the beam top and bottom flanges of the (a) CFS2-4-SP4#24, (b) CFSRuC2-4-SP4#24 and (c) CFS3-4-SP4#36 connections.

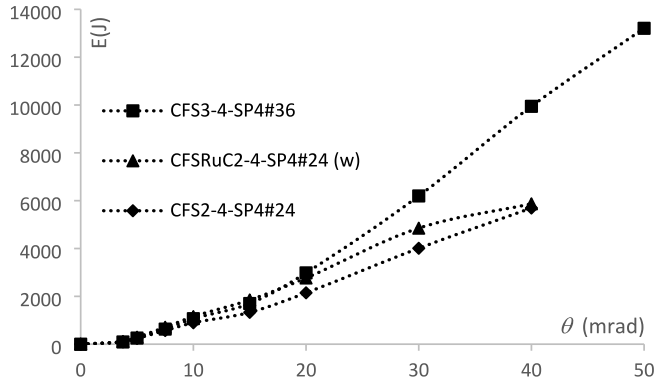

Fig. 9. Cumulative energy dissipation capacity of the CFS2-4-SP4#24, CFSRuC2-4-SP4#24 and CFS3-4-SP4#36 connections.

surrounded by their respective hysteretic curves. The use of infill RuC has boosted the energy dissipation of the CFSRuC2-4-SP4#24 (w) composite connection compared with that of the CFS2-4-SP4#24 bare steel connection up to 21 % at 30 mrad rotation. This, however, has been reduced to 3 % at 40 mrad rotation. As can be realised, the improvement in energy dissipation capacity of the composite connection using the infill RuC might not be deemed as significant particularly at the rotation corresponding to the connection failure (i.e., $\theta = 40$ mrad). The reason being the pinching nature of the hysteretic behaviour of the composite connection dominated by the screw shear limit state and its sharper strength degradation over the CD region (see Fig. 6) compared with a wider hysteretic curve of the CFS2-4-SP4#24 bare steel connection governed by the beam local buckling. The energy dissipation for the CFS3-4-SP4#36 bare steel connection (having 36 screw arrays), dominated by the side plate plasticity, has been increased by around 70 % compared with that of the CFSRuC2-4-SP4#24 (w) composite connection (having 24 screw arrays) at $\theta = 40$ mrad rotation. As can be seen in Fig. 9, the energy dissipation of the CFS3-4-SP4#36 connection has been further increased by 33 % at $\theta = 50$ mrad rotation compared with that at $\theta = 40$ mrad rotation. This indicates a side plate plasticity could be a more desirable energy dissipation mechanism than screw shear and beam local buckling mechanisms.

3.4. Connection rigidity

To assess the semi-rigid joint classification based on Eurocode 3-part 1-8 [25], the initial elastic stiffness of the bare steel and composite connections have been compared with the specified values for the simple and rigid joints. The boundary values are $S_{j,ini} = 0.5\ EI_b / L_b$ and $25\ EI_b / L_b$ for simple and rigid joints, respectively where EI_b and L_b are the

bending rigidity and the length of the beam. A joint is classified as semi-rigid when its elastic stiffness lies between these boundary values. Fig. 10 shows the relative beam-column rotation of both the bare steel and composite connections, calculated using $(D_1\text{-}D_2)/d$ (see Fig. 3), versus the bending moment at the connection centroid (M_c) corresponding to the elastic region in the hysteretic curves (i.e., region AB in Fig. 6). As can be seen all the bare steel and composite connections can be classified as semi-rigid joints, as their rigidity curves are fallen within that region. The CFSRuC2-4-SP4#24 composite connection, however, produces a greater initial rigidity by 3.4 times than that of the CFS2-4-SP4#24 bare steel connection. The reason being the connection screws of the composite connection were restrained by the infill RuC which has been resulted in a higher local stiffness for the screws. This restraining effect, however, has been reduced due to the bearing action of the screws against the plates and the surrounding concrete by increasing the loading cycles. A greater initial rigidity, in the same range as that of the composite connection, can also be achieved for the CFS3-4-SP4#36 bare steel connection by increasing the number of side plate screws from 24#12 to 36#12. As can be seen in Fig. 10, the initial connection stiffness of all the connections was gradually faded by increasing the connection rotation and progression of the plastic behaviour within the connection components.

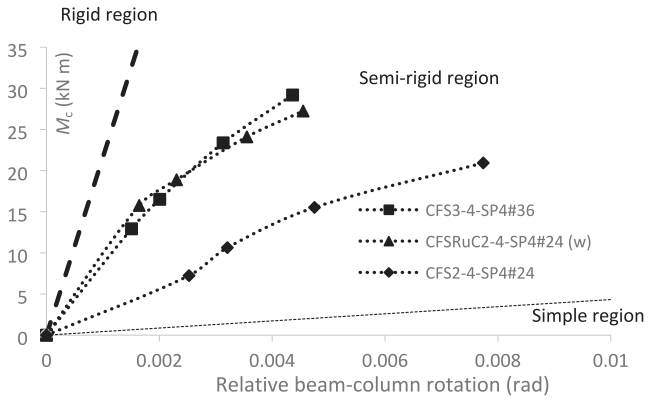

Fig. 10. Connection rigidity of the composite and bare steel connections.

4. Conclusions

By means of full-scale physical tests, a composite cold-formed steel (CFS)-Rubberised concrete (RuC) moment-resisting beam-to-column connection has been investigated under cyclic loading for seismic application. The beam and column sections were built-up using unlipped CFS channels attached to one another to form a tubular hollow section. The beam and column hollow sections were then filled with rubberised concrete (RuC) for the composite connection. The beam sections had either 2 mm or 3 mm thicknesses connected to a 4 mm thickness column through 4 mm thickness side plates. The side plates were welded to the column and screwed to the beam sides using 24 or 36 arrays of screws (forming CFS2-4-SP4#24, CFS3-4-SP4#36 bare steel and CFSRuC2-4-SP4#24 composite connections). The cyclic loading has been applied to the beam end through a loading actuator until the connection failure associated with a significant strength degradation has been reached.

The predominant failure limit states for the CFS2-4-SP4#24 and CFS3-4-SP4#36 bare steel connections were the beam local buckling and side plate plasticity, respectively, while the CFSRuC2-4-SP4#24 composite connection was failed due to the screw shear limit state. It was shown that the beam local buckling was effectively prevented by the infill RuC led to 45 % and 21 % higher moment strength and energy dissipation capacity, respectively, for the composite connection than those of the CFS2-4-SP4#24 bare steel connection. The boost in the energy dissipation capacity was not as significant due to the pinching nature of the hysteretic curve of the composite connection because of the screw shear failure and its sharper strength degradation. By increasing the number of screws from 24 to 36 the energy dissipation has been improved by 70 % for the CFS3-4-SP4#36 bare steel connection, dominated by side plate plasticity, compared with that of the composite connection. As a result, the side plate plasticity could be considered as a more favourable energy dissipation mechanism than the beam local buckling and screw shear energy dissipation mechanisms.

Both the bare steel and composite connections can be classified as semi-rigid joints as per the Eurocode 3-part 1-8 criteria. The composite connection produced a rigidity of up to 3.4 times greater than that of the CFS2-4-SP4#24 bare steel connection due to the restraining effect of the infill concrete surrounding the connection screws. A greater connection stiffness, comparable with that of the composite connection, has also been achieved for the CFS3-4-SP4#36 bare steel connection through the increased number of screws.

The test results presented in this research can be used for FE validation purposes to further investigate and extend the range and applicability of the proposed CFS-RuC connections in multi-storey construction through a parametric FE study on various connection configurations.

CRediT authorship contribution statement

Alireza Bagheri Sabbagh: Conceptualization, Methodology, Validation, Formal analysis, Investigation, Resources, Writing – original draft, Supervision, Project administration, Funding acquisition. **Naeimeh Jafarifar:** Conceptualization, Methodology, Validation, Formal analysis, Investigation, Resources, Writing – review & editing, Supervision, Project administration, Funding acquisition. **Paul Davidson:** Investigation, Writing – review & editing, Supervision. **Kanan Ibrahimov:** Investigation, Formal analysis, Writing – original draft.

Declaration of Competing Interest

The authors declare that they have no known competing financial interests or personal relationships that could have appeared to influence the work reported in this paper.

Data availability

Data will be made available on request.

Acknowledgement

This research was supported by the Royal Academy of Engineering Frontiers of Development Seed Funding scheme (FoD2021\4\26). Laboratory assistance from MSc student Callum Clark and laboratory and workshop technicians at the University of Aberdeen was much appreciated. The fourth author is grateful to the Ministry of the education of the republic of Azerbaijan for their financial support.

Disclaimer

Any opinions, findings, and conclusions or recommendations expressed in this publication are those of the authors and do not necessarily reflect the views of the sponsors and employers.

References

[1] The institution of Structural Engineers, IStructE, 2021, v99, 7.
[2] Hough MJ, Lawson RM. Proceedings of the institution of civil engineers. Civ Eng 2019;172(6):17–44.
[3] Madsen RL, Nakata N, Schafer BW. CFS-NEES Building Structural Design Narrative, Research Report, RR01; 2011, access at www.ce.jhu.edu/cfsnees.
[4] Ayhan D, Schafer BW. Cold-formed steel ledger-framed construction floor-to-wall connection behaviour and strength. J Constr Steel Res 2019;156:215–26.

[5] Bagheri Sabbagh A, Torabian S. Semi-rigid floor-to-wall connections using side-framed lightweight steel structures: concept development. Thin-Walled Struct 2021;160:107345. https://doi.org/10.1016/j.tws.2020.107345.
[6] Bagheri Sabbagh A. Cold-formed steel elements for earthquake resistant moment frame buildings, PhD thesis, University of Sheffield; 2011.
[7] Bagheri Sabbagh A, Petkovski M, Pilakoutas K, Mirghaderi R. Ductile moment-resisting frames using cold-formed steel sections: an analytical investigation. J Constr Steel Res 2011;67(4):634–46.
[8] Bagheri Sabbagh A, Petkovski M, Pilakoutas K, Mirghaderi R. Development of cold-formed steel elements for earthquake resistant moment frame buildings. Thin-Walled Struct 2012;53:99–108.
[9] Bagheri Sabbagh A, Petkovski M, Pilakoutas K, Mirghaderi R. Experimental work on cold-formed steel elements for earthquake resilient moment frame buildings. Eng Struct 2012;42:371–86.
[10] Bagheri Sabbagh A, Petkovski M, Pilakoutas K, Mirghaderi R. Cyclic behaviour of bolted cold-formed steel moment connections: FEM including slip. J Constr Steel Res 2013;80:100–8.
[11] Shahini M, Bagheri Sabbagh A, Davidson P, Mirghaderi R. Improving inelastic capacity of cold-formed steel beams using slotted blotted connection, In: International Specialty Conference on Cold-Formed Steel Structures, CCFSS 2018 (St. Louis, Missouri), USA; 2018.
[12] Shahini M, Sabbagh AB, Davidson P, Mirghaderi R. Development of cold-formed steel moment-resisting connections with bolting friction-slip mechanism for seismic applications. Thin-Walled Struct 2019;141:217–31.
[13] Shahini MF, Bagheri Sabbagh A, Davidson P, Mirghaderi R, Torabian S. Experiments on cold-formed steel moment-resisting connections with bolting friction-slip mechanism. J Constr Steel Res 2022;196:107368. https://doi.org/10.1016/j.jcsr.2022.107368.
[14] Eurocode 8: Design of structures for earthquake resistance. Part 1, General rules, seismic actions and rules for buildings. BS EN 1998-1: 2004.
[15] ANSI/AISC 341-05, 2005, Seismic Provisions for Structural Steel Buildings, American Institute of Steel Construction (AISC), Illinois.
[16] Ye J, Mojtabaei SM, Hajirasouliha I, Shepherd P. Seismic performance of cold-formed steel bolted moment connections with bolting friction-slip mechanism. J Constr Steel Res 2019;156:122–36.
[17] Ye J, Mojtabaei SM, Hajirasouliha I, Pilakoutas K. Efficient design of cold-formed steel bolted-moment connections for earthquake resistant frames. Thin-Walled Struct 2020;150:105926.
[18] Mojtabaei SM, Hajirasouliha I, Ye J. Optimisation of cold-formed steel beams for best seismic performance in bolted moment connections. J Constr Steel Res 2021; 181:106621. https://doi.org/10.1016/j.jcsr.2021.106621.
[19] McCrum DP, Simon J, Grimes M, Broderick BM, Lim JBP, Wrzesien AM. Experimental cyclic performance of cold-formed steel bolted moment resisting frames. Eng Struct 2019;181:1–14.
[20] Bagheri Sabbagh A, Jafarifar N, Deniz D, Torabian S. Development of composite cold-formed steel-rubberised concrete semi-rigid moment-resisting connections. Structures 2022;40:866–79.
[21] AISI-S100-16. North American Specification for the Design of Cold-Formed Steel Structural Members. Washington, D.C.: American Iron and Steel Institute; 2016.
[22] Li Z, Schafer BW. Buckling analysis of cold-formed steel members with general boundary conditions using CUFSM: conventional and constrained finite strip methods. In: Proceedings of the 20th International Speciality Conference on Cold-Formed Steel Structures, St. Louis, MO; 2010.
[23] Thai H-T, Uy B, Khan M, Tao Z, Mashiri F. Numerical modelling of concrete-filled steel box columns incorporating high strength materials. J Constr Steel Res 2014; 102:256–65.
[24] Tao F, Chatterjee A, Moen CD. Monotonic and Cyclic Response of Single Shear Cold-Formed Steel-to-Steel and Sheathing-to-Steel Connections. Virginia Tech Report No. CE/VPI-ST-16-01; 2016.
[25] Eurocode 3: Design of steel structures: Part 1.8: Design of joints, BS-EN 1993-1-8; 2005.